

---

This is an electronic reprint of the original article.  
This reprint may differ from the original in pagination and typographic detail.

Que, Zaiqing; Ahonen, Matias; Virkkunen, Iikka; Nevasmaa, Pekka; Rautala, Paavo; Reinvall, Hannu

## Study of cracking and microstructure in Co-free valve seat hardfacing

*Published in:*  
Nuclear Materials and Energy

*DOI:*  
[10.1016/j.nme.2022.101202](https://doi.org/10.1016/j.nme.2022.101202)

Published: 01/06/2022

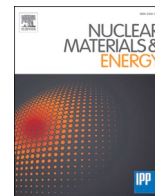
*Document Version*  
Publisher's PDF, also known as Version of record

*Published under the following license:*  
CC BY-NC-ND

*Please cite the original version:*  
Que, Z., Ahonen, M., Virkkunen, I., Nevasmaa, P., Rautala, P., & Reinvall, H. (2022). Study of cracking and microstructure in Co-free valve seat hardfacing. *Nuclear Materials and Energy*, 31, Article 101202. <https://doi.org/10.1016/j.nme.2022.101202>

---

This material is protected by copyright and other intellectual property rights, and duplication or sale of all or part of any of the repository collections is not permitted, except that material may be duplicated by you for your research use or educational purposes in electronic or print form. You must obtain permission for any other use. Electronic or print copies may not be offered, whether for sale or otherwise to anyone who is not an authorised user.



## Study of cracking and microstructure in Co-free valve seat hardfacing

Zaiqing Que<sup>a,\*</sup>, Matias Ahonen<sup>a</sup>, Iikka Virkkunen<sup>b</sup>, Pekka Nevasmaa<sup>a</sup>, Paavo Rautala<sup>c</sup>, Hannu Reinvald<sup>a</sup>

<sup>a</sup> Nuclear Reactor Materials, VTT Technical Research Centre of Finland, Kivimiehentie 3, FI-02044 VTT, Finland

<sup>b</sup> Department of Mechanical Engineering, Aalto University School of Engineering, Otakaari 4, 02150 Espoo, Finland

<sup>c</sup> Teollisuuden Voima Oyj, 27160 Eurajoki, Finland

### ARTICLE INFO

#### Keywords:

Hardfacing  
Cobalt-free  
Valve  
Nuclear  
Microstructure

### ABSTRACT

For reducing the radiological hazard, Co-free hardfacing alternatives have been used to replace the traditional Co-based hardfacing alloys in nuclear power plant applications. However, manufacturing a defect-free Co-free hardfacing is challenging. Reduced galling resistance and mechanical properties exhibited by common replacement alloys in some conditions limit the application. This issue is important for the operating nuclear power plants with lifetime extension and also for the new builds. In this paper, a failed industrial hardfacing was studied. Through-the-thickness cracks of the Co-free hardfacing deposit with NOREM 02 on a nuclear swing check plug were detected. The potential cause of the brittle interdendritic cracking was studied and the detailed microstructure of the Co-free hardfacing analysed. The solidification defects during the manufacturing and the lacking of ferrite phase in the microstructure together with the potentially non-optimized handling procedures are concluded to be the causes of the observed cracking.

### Introduction

Cobalt-based Stellite alloys have successfully been applied for decades for hardfacing applications on wear surfaces in valves, pumps, turbines, and control rod drive systems in nuclear power plant (NPP) applications, owing to their excellent wear and galling resistance and good weldability [1–3]. However, cobalt is a harmful element in the nuclear environment since the activation of cobalt-containing wear or corrosion debris in the primary circuit of the power plant can transform <sup>59</sup>Co to <sup>60</sup>Co and <sup>58</sup>Co and then these radioactive nuclides can spread from the reactor core region throughout the piping system, possibly resulting in a higher than necessary dose to the staff during outages and operation. High-cobalt alloys such as Stellites should be avoided for valve seat hardfacing materials in systems in contact with reactor coolant. The topic of Co-free hardfacings has been under active study and results on new alloys have been published for both nickel-base [4] (i.e. Tribaloy 700, Deloro and Colmonoy alloys) and iron-base [5,6] (i.e. Nitromaxx, NOREM 02 and Antinit DUR 300/500), and lately also additively manufactured coating, e.g., Vibenite [7].

The replacement of Co-based hardfacing alloys in the NPPs is an important issue as part of the continuous efforts to minimize radiological contamination and improve the radiation safety. The topic is also critical

for the new NPP builds, where the choice of hardfacing alloys for the valves requires to be made possibly even on an individual valve basis, with the target to minimize the utilization of Co-based hardfacings. NOREM 02 and the Antinit DUR 300 alloys are among the most common Co-free hardfacing alloys used in the nuclear industry at the moment with adequate wear and galling resistance in some conditions [1,8,9], particularly for new builds, modernisation and replacements. However, early indications of subsurface defects during welding are sometimes found, mostly due to their low ductility and lack of plastic deformation capability and the coatings suffer from increased wear rates in operational temperatures [10–12]. Manufacturing a defect-free Co-free hardfacing is challenging, even though strategies like controlling the welding parameters (e.g. heat input, interpass temperature, pre-heating, cooling rate and post-weld heat treatment), choice of welding process (e.g. beam-like processes: laser beam welding LBW, plasma transferred arc welding PTAW vs. arc-welding processes: gas metal arc welding GMAW, gas tungsten arc welding GTAW, shielded metal arc welding SMAW), welding technique (e.g. number of layers/passes, layer thickness and hardfacing thickness) and alloying adjustments to improve the weldability [4,9,11] have been investigated for producing crack-free welds and enhancing the hardfacing integrity. With crack formation and propagation in hardfacings during manufacturing and operation, the

\* Corresponding author.

E-mail address: [zaiqing.que@vtt.fi](mailto:zaiqing.que@vtt.fi) (Z. Que).

<https://doi.org/10.1016/j.nme.2022.101202>

Received 23 November 2021; Received in revised form 19 May 2022; Accepted 20 May 2022

Available online 21 May 2022

2352-1791/© 2022 The Authors. Published by Elsevier Ltd. This is an open access article under the CC BY-NC-ND license (<http://creativecommons.org/licenses/by-nc-nd/4.0/>).

**Table 1**

The chemical composition of the NOREM 02 hardfacing.

Elements	Fe	Cr	Mn	Ni	Si	Mo	C	N	Co
wt. %	Balance	24.0	4.5	4.1	3.3	2.0	1.27	0.16	0.02

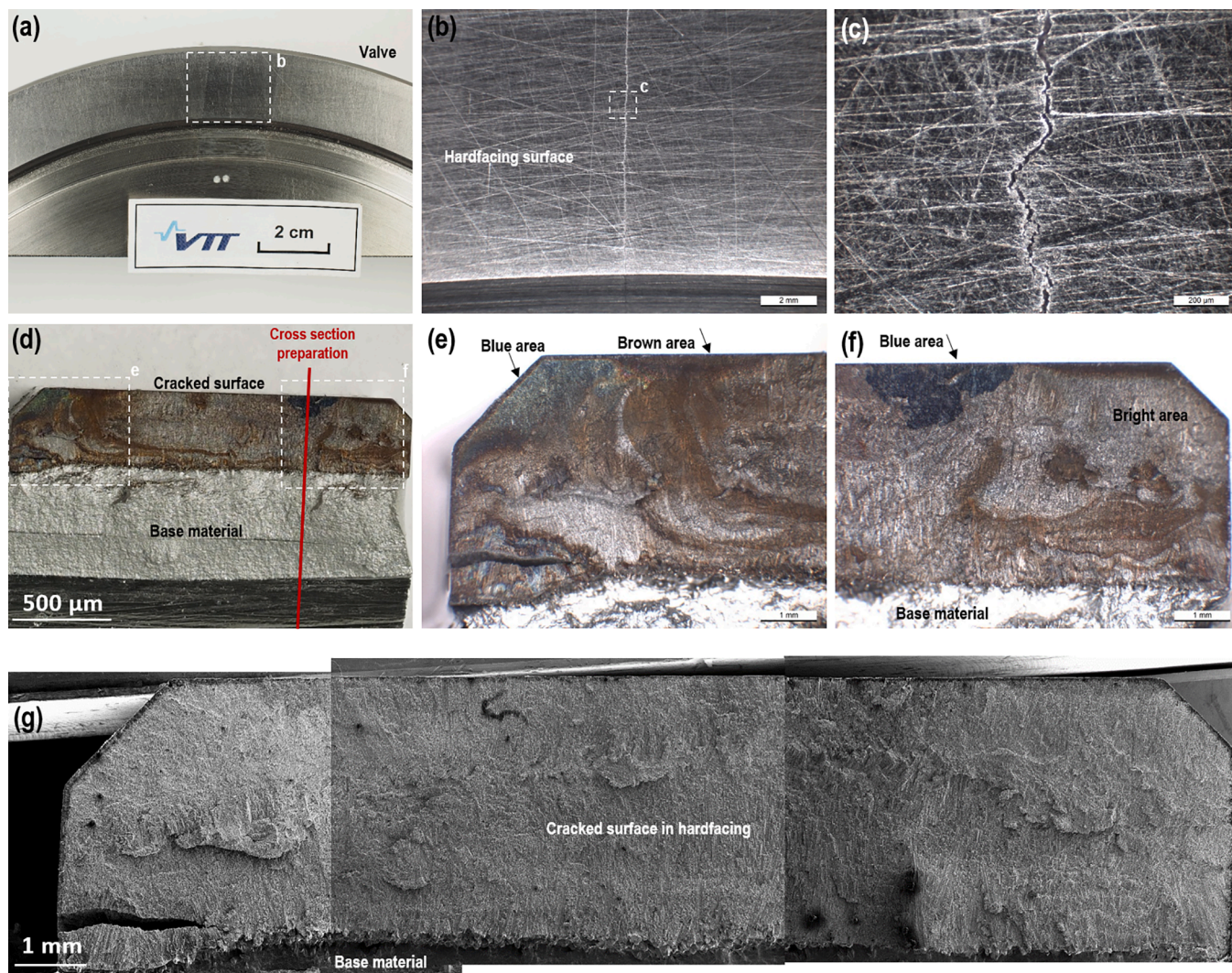


**Fig. 1.** (a) Photograph showing the appearance of the valve piece in as-received condition. (b-c) Stereomicroscope images of the crack in the hardfacing, depicted from the upper surface of the valve. The crack is straight and axial (radial). (d-f) Optical images showing the fracture surface of the cracked hardfacing. The hardfacing is in the upper part of the picture. The crack covers the whole hardfacing, and the part with metallic appearance is the stainless steel base material, formed during the opening of the crack. Blue, brown and metallic bright areas were seen in the hardfacing. (g) Overview of the cracked NOREM 02 hardfacing surface under SEM.

risk of debris detaching from the surface and ending up in the primary system is increased. In the worst case, such loose particles may cause fuel rod damage and a subsequent fuel leakage, which is jeopardizing the operation of the reactor, possibly causing an un-planned outage and, at worst case, a release of fission products to the primary water. However, publicly available information on the status and behaviours of these Co-free alloys subject to service conditions in the NPPs is rather limited.

With a high hardness and ultimate tensile strength but low fracture elongation and limited wear resistance at elevated temperatures, NOREM 02 is normally used as a substitute for Co-based hardfacing in nuclear stop and swing check valves, globe valves and butterfly valves [13,14]. Grand Gulf Nuclear Station used NOREM in the in-situ repair of two 24" feedwater check valves in 90 s [15]. A large number (>400) of

replacement valves with NOREM trim have been applied onto operating light water reactors before 2000 [16]. Two 1.5" 1500# class globe valves installed in the chemical volume control system at Union Electric's Callaway Nuclear station suffered significant damage following one 18 month operating cycle [17]. However, detailed examination of the discharged disc was reported as impossible [17]. The comprehensive understanding of the microstructure in nuclear valve hardfacing in addition to that from model alloys or weldability study is still lacking. Furthermore, the knowledge of the potential cracking mechanisms for the NOREM 02 hardfacing applied on nuclear valves is still insubstantial.

This study is based on the investigations of one cracked NPP swing check valve plug. This work aims to investigate the potential cause of the through-the-thickness cracking of the hardfacing deposit made from

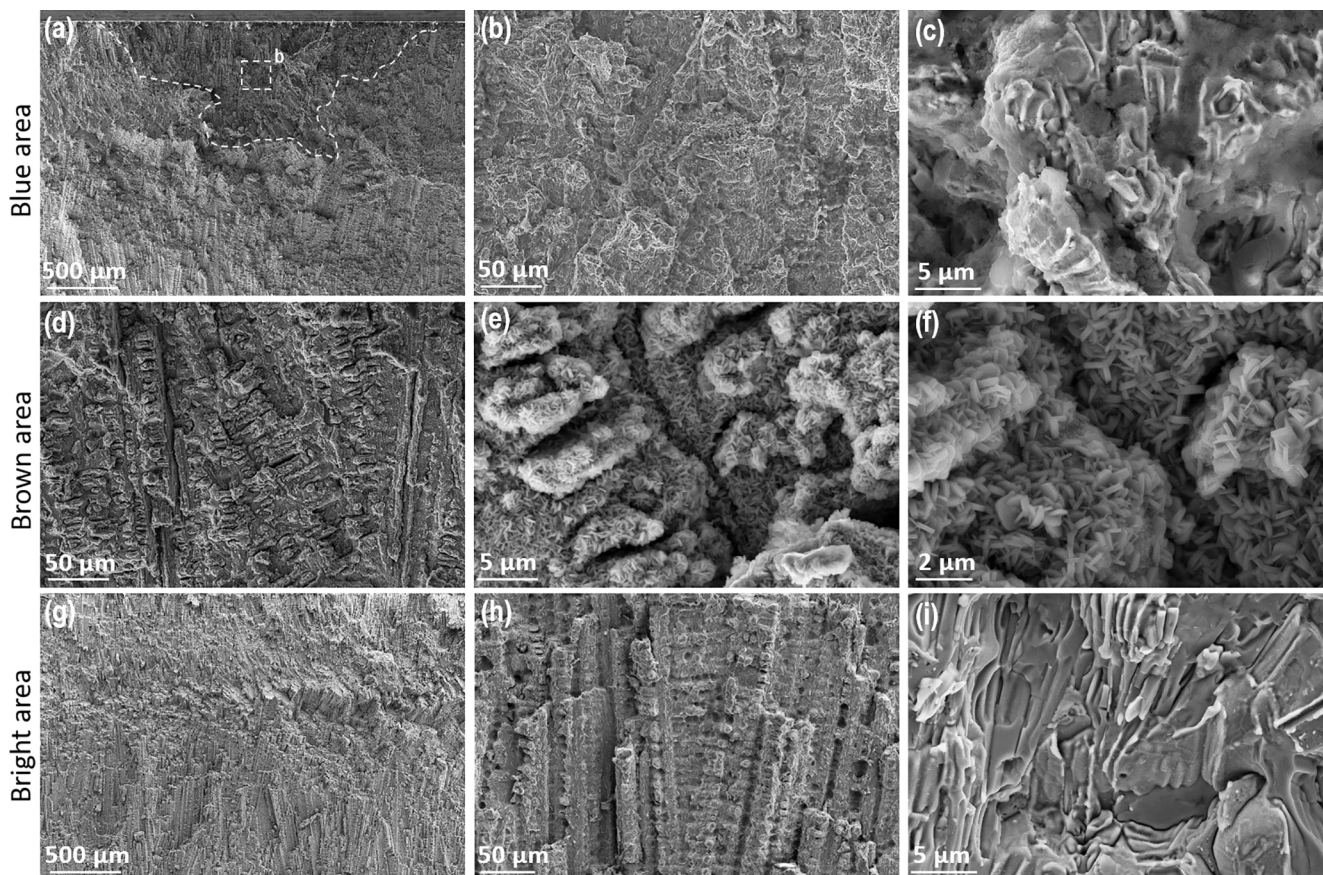


Fig. 2. (a-c) SEM-SE images showing the area, which appears as blue area in the optical photograph of the fracture surface. Thick and discontinuous oxide layer was observed on the blue area of fracture surface. (d-f) SEM images of the brown area of the fracture surface. The fracture surface is dendritic. A large amount of sub-micron needle- and flake-like oxide particles, covering the fracture surface almost completely in the brown area. (g-i) SEM images of the metallic bright area of the fracture surface. Pure brittle features along the dendritic microstructure were observed.

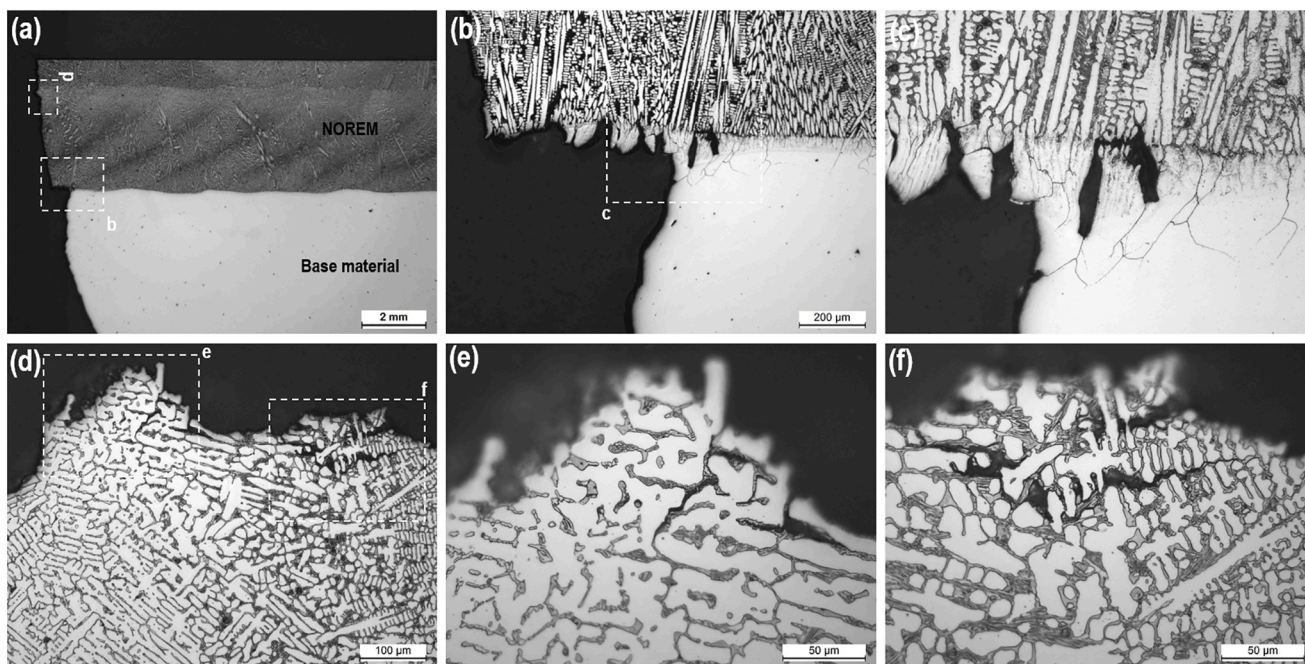


Fig. 3. (a-f) Optical micrograph of the cross-section in etched condition. (a) The weld beads seem to be about 1 mm thick in the main part of the hardfacing. The top layer has been welded separately. (b) On this side of the opened piece, the stainless steel is missing from about 0.6 mm long portion of the cross-section next to the crack. (e-f) Cracking occurs along the carbide structure.

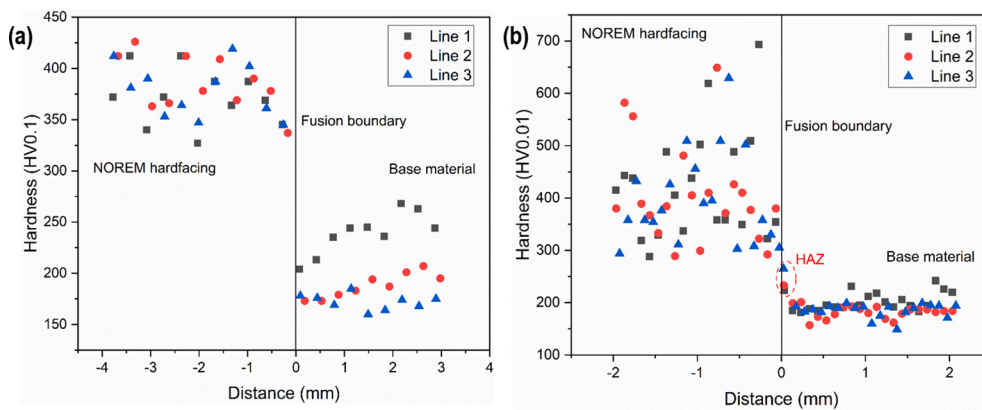


Fig. 4. (a) HV0.1 Line 1 - Line 3 and (b) HV0.01 Line 1 - Line 3 across the fusion boundary between the NOREM 02 hardfacing and base material.

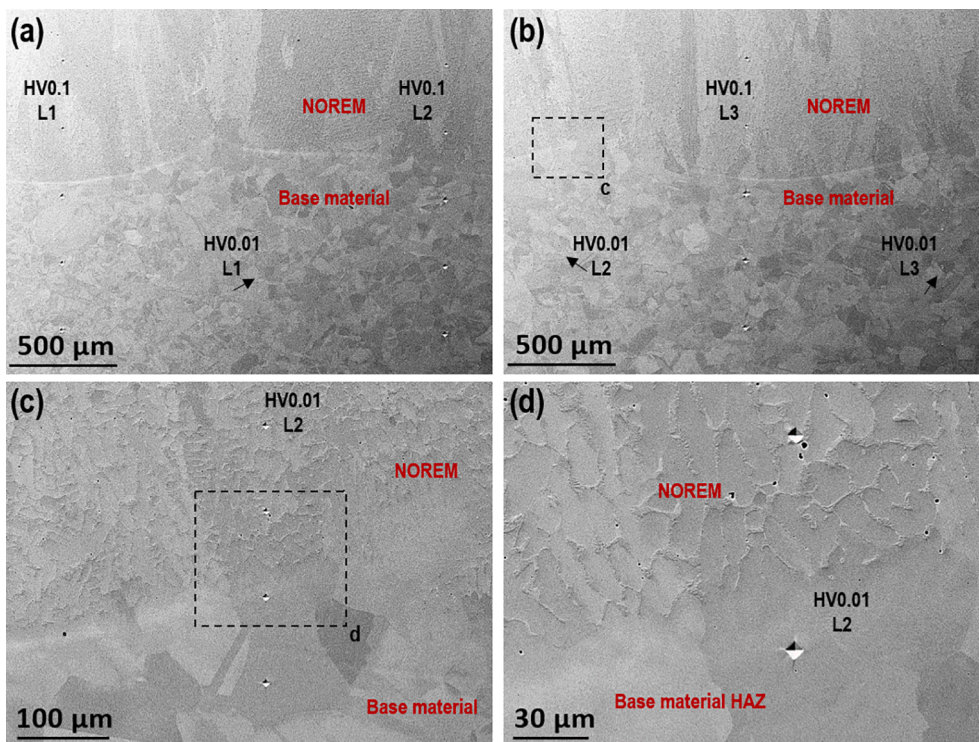


Fig. 5. (a-d) SE images showing the HV0.1 L1-L3 and HV0.01 L1-L3 across the fusion boundary between the NOREM 02 hardfacing and 316L base material. The HV0.01 has a smaller indent spacing and smaller indent size compared to the HV0.1.

NOREM 02 and analyse the detailed microstructure of the Co-free hardfacing to understand the microstructural factors contributing to the cracking. The caution of application and the corresponding potential mitigation methods are proposed.

**Experimental**

*Material*

NOREM 02 as powder metallurgical filler metal was applied on parts of the swing check valve through PTAW process on a stainless steel 316L valve body. After deposition, a stabilisation post-weld heat treatment at 500 °C/4h was performed. The chemical composition of the studied NOREM 02 is listed in Table 1. After the final machining of the valve, a dye penetrant test was performed on the top surface of the valve hardfacing. No reportable indication of cracking was detected by the manufacturer and the valve was reported to fulfill the allowed internal

leak rate criteria. Therefore, the factory acceptance test for the valve was passed. The investigated valve has been part of safety injection system for a very short period of operation in cold condition in the NPP. When the valve was opened for inspection a radial crack across the sealing surface was observed in the hardfacing.

The NOREM 02 has good general corrosion resistance because of its high contents of chromium and molybdenum. The yield strength and ultimate tensile strength of NOREM 02 is 675 and 900 MPa at room temperature, respectively. NOREM 02 exhibits low fracture elongation (~0.6–2 %) at room temperature. The average hardness of NOREM 02 is 39–40 HRC.

*Investigations*

Both the fracture surface and the axial cross section of the cracked valve were studied. A V-shaped notch in the valve body (stainless steel 316L) was machined to be as close as possible to the hardfacing (Fig. 1)

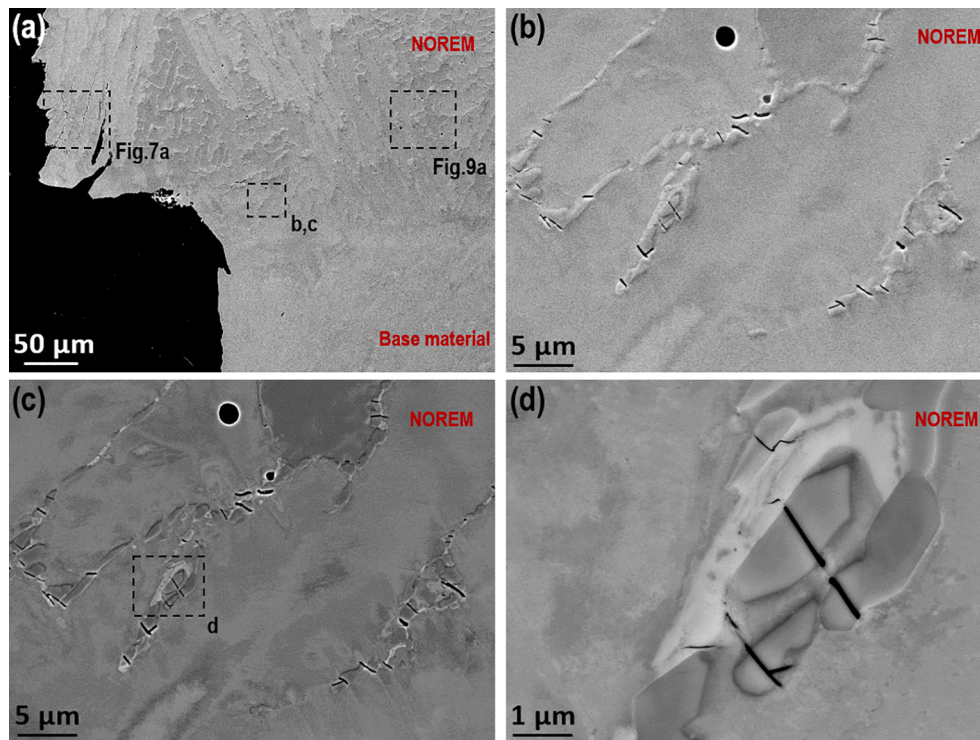


**Fig. 6.** (a–b) SE images and (c–d) BSE images of cracked carbides in the NOREM O2 hardfacing at locations close to the main cracked surface and fusion boundary between the hardfacing and the base material.

and bent open to minimise the size of the remaining ligament and thus facilitate the opening of the crack with as little plastic deformation as possible. The specimen was then sectioned parallel to the axial direction (perpendicular to the cracked plane). The cross section was studied in both etched and fine-polished conditions. The last step of the surface preparation of the fine-polished cross section specimen was with a non-crystallizing amorphous colloidal silica suspension (0.04 µm).

The fracture surface of the opened crack and the cross section were investigated with stereomicroscope, light optical microscope and scanning electron microscopy (SEM). A Zeiss Crossbeam 540 SEM equipped with a solid-state four-quadrant backscatter detector (BSD) and an EDAX Hikari Plus electron backscatter diffraction (EBSD) detector was used. The microstructure was investigated using SEM secondary electron (SE) and backscatter electron (BSE) imaging techniques. SE imaging was performed with high voltage mode and low voltage mode at respective working distances (WD). High voltage mode is conducted with 15 keV, 1.5nA and WD of 10–15 mm while low voltage mode is with 5 keV, 0.5nA and WD of 5–7 mm. High voltage mode is more sensitive to chemical composition difference (Z contrast) while low voltage mode more sensitive to surface layer topography (morphology contrast). BSE is based on the dependence of the backscatter electron signal on the orientation of crystal lattice planes with respect to incident electron beam due to electron channelling. BSE imaging was conducted at an accelerating voltage of 15 keV with a WD of 5–6 mm. EBSD mapping was conducted at an accelerating voltage of 20 keV and WD of 13–14 mm with 70° tilting and a probe current of 3 nA. EBSD image quality (IQ) maps, inverted pole figure (IPF), pole figures, kernel average misorientation (KAM) and phase maps were analysed by TSL OIM Analysis 8.1 software. For reducing the interaction volume of the incident electrons with the material (due to the sub-micron sizes of the carbides), Energy Dispersive X-Ray (EDX) with an accelerating voltage of 5 keV and a probe current of 1.5nA was applied. The microhardness measurements of HV0.1 and HV0.01 on the specimen cross section was performed with Durascan 80. HV0.1 and HV0.01 indents were performed with spacing of 0.35 and 0.1 mm, respectively.

## Result

### Fracture surface

A valve with sealing surface made from NOREM O2 hardfacing and valve body base material from austenitic stainless steel 316L, contained a crack over the whole width of the hardfacing (about 22 mm), as seen in the Fig. 1(a). The straight and axial (radial) crack has propagated through the full thickness of the hardfacing deposit (Fig. 1(b–c)). Cracks were limited to the NOREM O2 hardfacing layer (Fig. 1(d)) and did not propagate into the stainless steel base metal, which has a more ductile behaviour and a higher ductility than the NOREM O2 hardfacing material. Since such cracks were not detected during the dye penetrant testing performed by the manufacturer, they were not supposed to be present after short service time either.

The fracture surface is seen in the Fig. 1(d). Fracture surface in different colours (blue, brown and bright areas) were observed, as shown in Fig. 1(e–f). Two blue areas were clearly separated from the rest of the brownish fracture surface and they were in direct contact with the outer surface. The brown coloured areas covers the majority of the fracture surface until the fusion boundary between the hardfacing and the base material. Additionally, a radial crack of 2–3 mm detaching the weld and base material along the fusion boundary was found (lower left part in Fig. 1(e,g)).

The blue areas, which have a clear border to the rest of the brownish fracture surface, resembles that of tempering colours, mainly due to chromium oxides. Based on this, it seems most likely, that the blue areas have encountered high temperatures (*i.e.*, higher than during plant operation) and oxygen in the environment. Therefore, it seems likely that these blue areas have formed during the manufacturing of the hardfacing, either during welding or cooling of the weld, or during the stabilisation heat treatment. The brown colour forms curved patterns, with the imaginary centre being on the sealing surface. That indicates that these brown areas have also been in contact with an oxygen-containing atmosphere. It is probable that these brown areas had

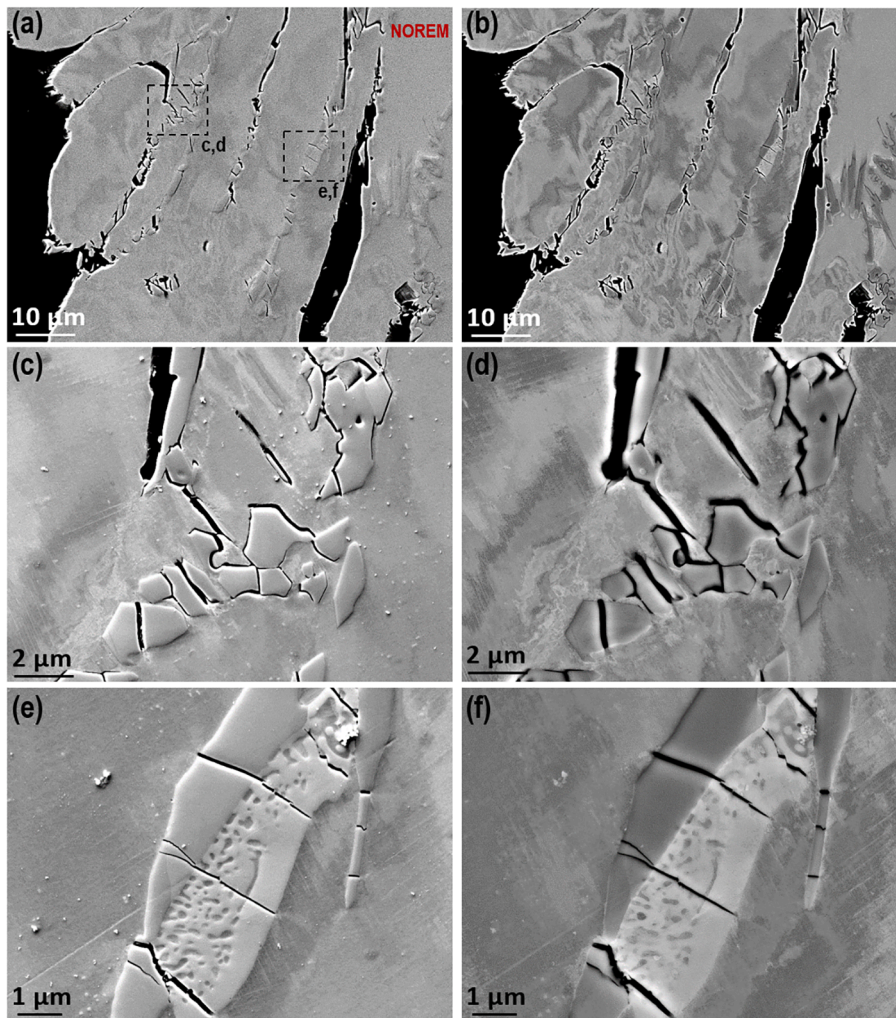


**Fig. 7.** (a,c,e) low kV SE images and (b,d,f) BSE images of the same areas with cracked carbides in the NOREM O2 hardfacing. The area investigated was from Fig. 6 (a). The cracking followed the ID network of cracked carbides in the NOREM O2 hardfacing.

contact with air at the lateral side of the deposit (internal or external diameter) of the hardfacing material other than the sealing surface of NOREM O2 deposit. There are also bright areas, which are free from additional colouring and oxides, but resemble as uncracked ligament with a fresh, metallic and oxide-free fracture surface. The macroscopic appearance of the fracture surface (Fig. 1(d,g)) indicates that the crack has initiated at different locations (blue areas), and grown from these and coalesced into the final crack (brown areas).

The SEM investigations in Fig. 2 revealed that the general fracture surface has a brittle dendritic appearance. The fracture surface of the blue area (Fig. 2(a-c)) does not differ substantially from the overall surrounding area, other than by having denser oxide on the fracture surface. The surface is covered by a solid but discontinuous oxide layer (Fig. 2(c)). The brown area has a similar surface appearance in SEM as the other areas, concerning the dendritic morphology of the fracture surface and the overall appearance (Fig. 2(d-f)). However, at a larger magnification it clearly shows a different appearing oxide structure with distinctly formed oxide needles (Fig. 2(f)). No significant signs of weld defects, such as hot cracks, were observed in the blue or brown areas on the fracture surface, which could be due to the covering of the fine details by the oxide structure. EDX reveals a higher oxygen content in blue area than in the brown area and the Fe/Cr ratios are 1.5 and 4.5 in the blue and brown areas, respectively, indicating a different compositions of the oxides covering the surfaces. The bright areas exhibits a dendritic

solidification structure without oxide layer (Fig. 2(g-i)).

#### Cross-sectional investigation

Based on the visual inspection of the broken half, the depth of the crack along the fusion line varies slightly along the hardfacing width. A cross-section was prepared from the location with a blue area next to the outer surface of the hardfacing (cutting location shown in Fig. 1(d)). The cross-section was investigated using a light optical microscope in etched condition and by SEM in fine-polished condition. The thickness of the coating varies between 3.9 and 4.1 mm (Fig. 3(a)). As revealed in Fig. 3 (a), the weld beads are about 1 mm thick in the bottom part of the hardfacing and have been welded along the circumference of the valve seat. The top layer(s) of the hardfacing is about 0.7 mm thick, and has been welded on top of the bottom layers. A 0.6 mm long portion along the fusion line of the stainless steel valve body material is missing next to the main crack, which was due to the crack growth along the fusion line of the hardfacing. The cracking did not extend into the valve body material (Fig. 3(b-c)). The microstructure at the interface between the top and bottom hardfacing beads is shown in Fig. 3(d). The microstructure of the top layer of the hardfacing is finer, *i.e.*, the dendrites are smaller in the top layer bead (Fig. 3(f)) compared to the bottom beads (Fig. 3(e)). Furthermore, there appears to be more continuous carbides in the top layer based on the macroscopic appearance. It is worth

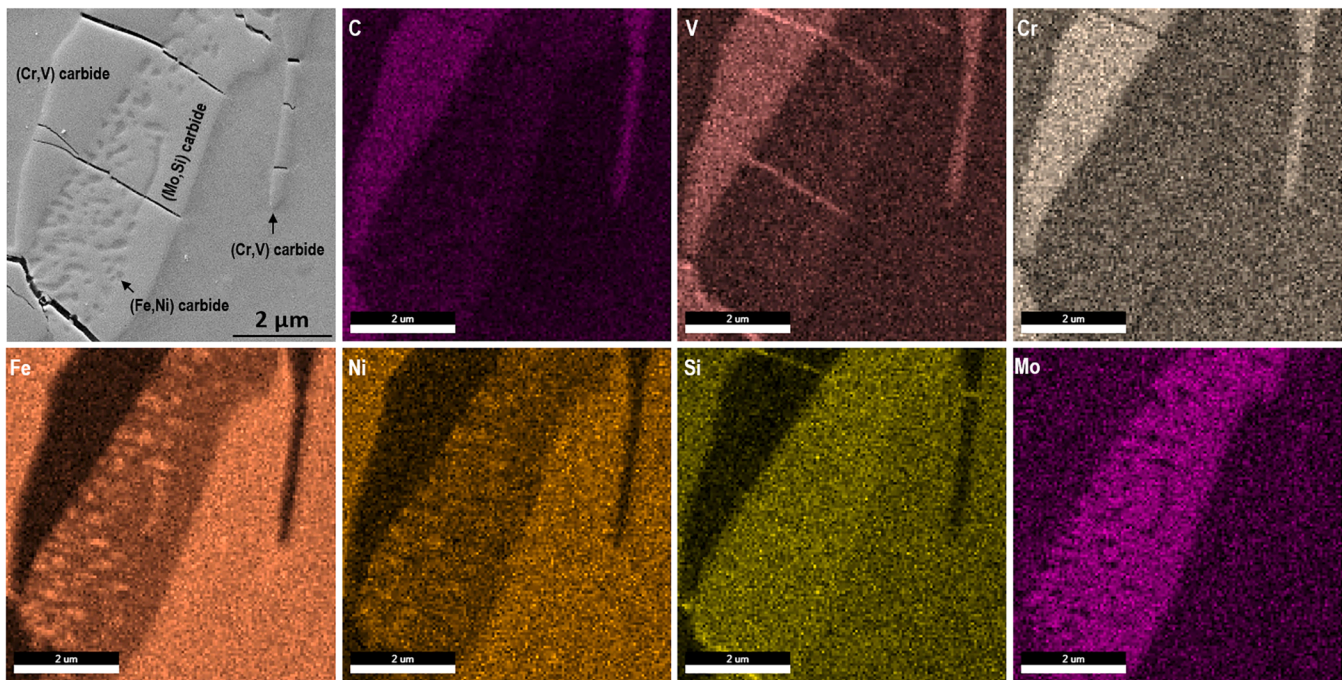


Fig. 8. EDX mappings of the cracked carbides for the area in Fig. 7(e). The chemical compositions of the eutectic and non-eutectic carbides were revealed.

mentioning that the blue area was found in the top bead layer. Interdendritic (ID) cracking occurs along the carbide structure (Fig. 3(e-f)).

The microhardness measurements data and the corresponding SE images of HV0.1 and HV0.01 across the NOREM 02 hardfacing-base material fusion boundary are shown in Fig. 4 and Fig. 5, respectively. As shown in Fig. 5(c-d), the NOREM 02 hardfacing has a dendritic microstructure while the base material 316L has a typical austenitic microstructure with equiaxed grains. The HV0.1 indents exhibit a more uniform microhardness in the NOREM 02 hardfacing part compared to HV0.01. This is due to that a smaller indent size of HV0.01 can hit either the ID carbides or the interior of the matrix in the fine dendritic microstructure of the hardfacing. When measuring the microhardness of base materials 316L, HV0.1 indents exhibit a higher scatter compared to HV0.01, which is because of that the majority of HV0.01 indents are within the austenitic grain interior while the HV0.1 has a bigger indent size and thus higher chance of hitting grain boundaries (GBs). Both HV0.1 and HV0.01 show the significant hardness difference across the fusion line (twice the average microhardness in hardfacing than the base material). Furthermore, microhardness of heat-affected zone (HAZ) of base material 316L was revealed in the Fig. 4(b) with a smaller indentation spacing of HV0.01 than HV0.1.

Detailed characterizations were performed for the locations next to the main crack and close to the fusion line, where the crack growth along the fusion line of the hardfacing was observed (Fig. 6(a)). As shown in Fig. 6(b-d), SE images and BSE images revealed the cracked ID carbides in the NOREM 02 hardfacing. This indicates that the ID carbides are more brittle and have lower resistance to cracking when subject to external loading compared to the hardfacing matrix. In the studied component, no *trans*-dendritic cracking was observed in the crack path in the hardfacing material. In Fig. 7, low kV SE images and high kV BSE images of the same areas from Fig. 6(a) showed that the ID cracking was associated with the cracked carbides in the NOREM 02 hardfacing. The cracks propagated and grew along the interface between the matrix and the cracked carbide and merged. The cracks propagated preferentially along the areas where the carbide structure is continuous, and some cracks seem to be arrested in locations of discontinuous carbide structure. Furthermore, the crack growth direction was parallel to the dendrite growth direction and the dendrite packages that were

perpendicular to the main stresses were found to be the most susceptible to cracking. Both eutectic and non-eutectic carbides in the ID networks were observed, as shown in Fig. 7(e-f). The eutectic part reveals large amounts of 150–300 nm carbide particles. The carbides in Fig. 7(e) were further investigated by EDX mappings in Fig. 8. The micron size eutectic carbide phase is mainly formed by Mo-Si rich precipitates and decorated with a large amount of nanometre size (Fe, Ni) carbides. The pre-deposited non-eutectic carbides are (Cr, V) carbides. In Fig. 9, low kV SE images and BSE images of the area from Fig. 6(a) close to the HAZ of the NOREM 02 hardfacing-base material fusion boundary revealed the presence of ID cavities. Since the studied area is further away from the main crack, there was no observation of cracked carbides. It was found that a high concentration of ID cavities was found within the HAZ induced by the 2nd bead of the hardfacing layer. This indicates that the hardfacing material has experienced sort of reduction in ductility at certain temperature range, which has led to the formation of ID cavities or ID decohesions. The clusters of ID cavities in the HAZ can easily join together by micro-cracks. In Fig. 9(e-f), the 3 categories of carbide were observed and some of the nanometre size carbide particles in the eutectic phase seem to be interconnected. ID decohesions were observed not only in the HAZ of weld beads in the hardfacing layer but also at the triple joint location of two weld beads in the NOREM 02 hardfacing-base material fusion zone boundary. As shown in Fig. 10, at the triple joint location the low kV SE images and BSE images reveals cracked carbide and iron phase lamella. It is worth mentioning that the metallographic (Fig. 3(d)) and fractographic SEM images (Fig. 7(a)) of the cross-sectional area close to the main crack surface showed cracking along the ID phases, while the discrete iron phase dendrites exhibit certain amounts of plastic deformation before their necking failure. The hardfacing matrix has a more ductile behaviour compared to the ID carbides.

The microstructure of representative intact NOREM 02 hardfacing material was comprehensively investigated from Fig. 11 to Fig. 14. The typical microstructure of solid-solution strengthened NOREM 02 hardfacing material consists of a dendritic austenitic matrix with ID network of carbides with M7C3 type (with very limited fraction of M23C6 type). Eutectic complex carbides rich in Fe-Mn-Ni and Mo-V-Si and non-eutectic carbides rich in Cr-V were found (Fig. 12). The chemical composition of the carbides varied slightly from the intact area to the

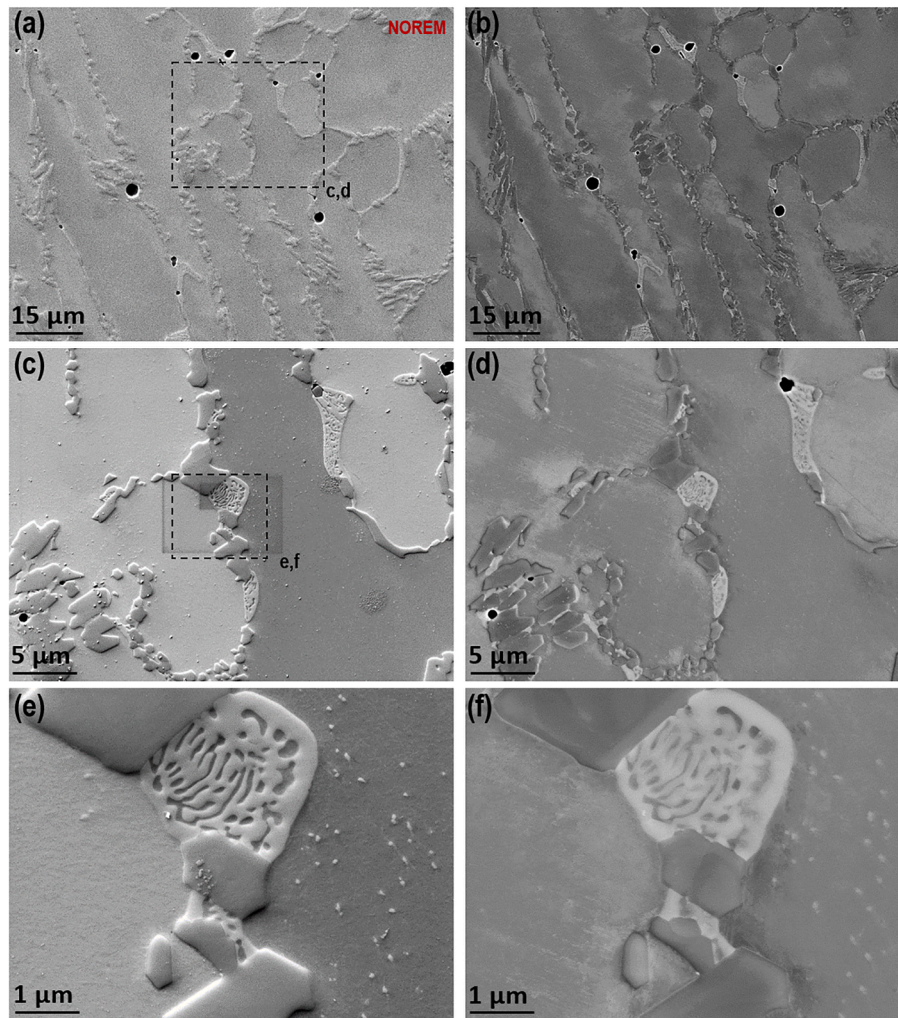


Fig. 9. (a,c,e) low kV SE images and (b,d,f) BSE images of the same areas close to the HAZ of the NOREM 02 hardfacing-base material fusion boundary. The area investigated was shown in Fig. 6(a). ID cavities were observed.

area close to the main crack, but the difference is reasonable taking into account the complex bead and solidification structure. IQ maps were based on the band contrast and thus a darker colour revealed a stronger deformation than the lighter region. KAM can be used to estimate geometrically necessary dislocation densities [18,19]. The IQ and KAM maps in Fig. 13 and Fig. 14 indicated a high lattice distortion and strong localization of strain at the ID network. The microstructure is highly textured and the columnar dendrites grow in the  $\langle 100 \rangle$  direction, as indicated by the pole figures from Fig. 13 and Fig. 14. The microstructure reported here are in general consistent with those reported by Ocken [17], Ohriner [20] and Cockeram [21]. However, there are several differences. In the literatures, some islets of ferrite have been reported to occur inside the austenitic matrix. These may form by fast cooling from high temperature during the welding process and may increase the dendrite yield strength and toughness, as well as improve the galling resistance. These ferrite island were not observed in the current investigated microstructure. In addition, the austenitic dendrites were smaller in size/volume compared in literature ( $\sim 10 \mu\text{m}$  vs  $\sim 50\text{--}100 \mu\text{m}$ ). Furthermore, the enrichment of elements in ID carbides and type of carbides varied from study to study. The slight differences in the observed microstructure with literature could have been induced by the alloying adjustments, deposition method and parameters.

## Discussions

### *The crack formation and propagation process*

As revealed by the fractographic investigations, a big portion of the cracks have been formed during the manufacturing (blue and brown areas). NOREM 02 hardfacing is assumed to experience a ductility drop at the manufacturing temperature range resulting from solidification cracking or hot cracking formed in the ID areas in a liquid state. Alloys like NOREM 02, which solidify with a primary austenitic structure can be susceptible to the solidification cracking, which is caused by low-melting point eutectics containing alloy elements such as Si, Ti, N and Nb and impurities such as P and S [22–24]. The solidification range and the crystallization of the final portion of the liquid phases concentrated with low-melting point impurities and alloying elements of NOREM 02 depends on the composition of the alloy [25].

The carbide cracking exhibits a characteristic morphology, where cracks form perpendicular to the long axis of the elongated carbide areas with roughly equal distance (Fig. 6 to Fig. 7). In most cases, the cracks show high opening and significant blunting. These features indicate that the dominating stress driving these cracks is the thermal contraction mismatch between the carbide and the surrounding matrix. This stress is effectively relieved by the observed cracking pattern. The significant blunting indicates, that many of these cracks form fairly early after solidification and blunt during further cooling. In addition, some sharp-

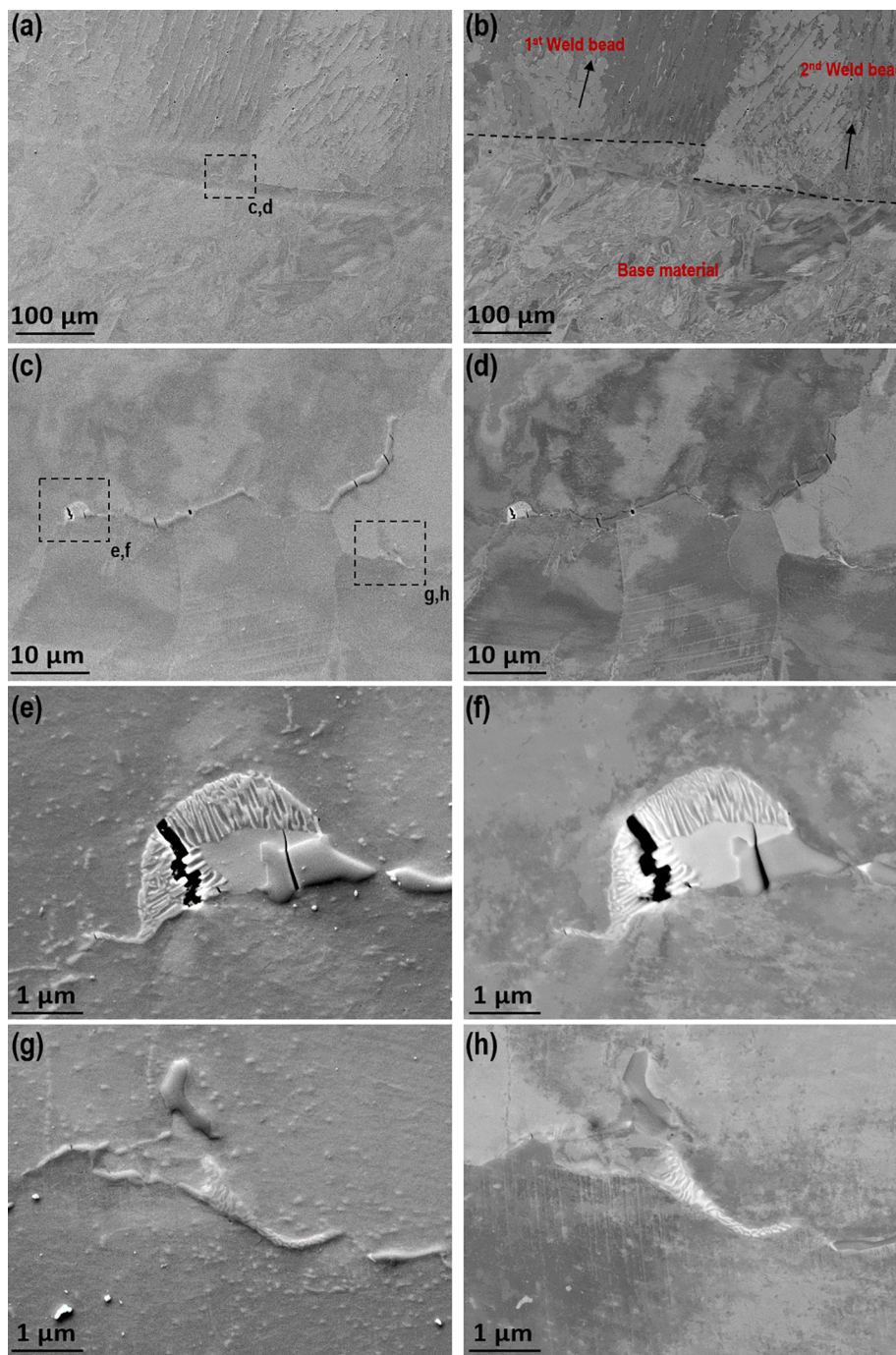


**Fig. 10.** (a,c,e,g) low kV SE images and (b,d,f,h) BSE images of the same areas at the triple joint location of two weld beads in the NOREM 02 hardfacing-base material fusion boundary. The images revealed cracked carbide and iron phase lamella.

tipped cracks were observed, which are assumed to have been formed later during cooling. During the manufacturing procedure of the valve, the solidification cracks can reach the lateral sides of the hardfacing material at relatively high temperatures and have a small contact with ambient air, which leads to the observed tempering oxidation. During valve installation and operation, the additional tensile loading together with the metallurgical defects in the NOREM 02 hardfacing deposit finally assist in the through-the-thickness cracking.

As shown in Fig. 3 and Fig. 7, the cracking occurs along the ID carbide structure where the hard and brittle carbide structure is continuous (the blue area in the top layer) and where the dendrite packages were more perpendicular to the main stresses. The hardfacing matrix has a

more ductile behaviour compared to the ID carbides and the dendrites exhibit certain amounts of plastic deformation before their necking failure. Micro-cracks can easily initiate at the ID networks result from the incompatible deformation between the hard carbide phases and the soft matrix under exterior load or stress. Higher geometrically necessary dislocation densities develop at the matrix-carbide interfaces, as indicated by the KAM mapping in Fig. 13 and Fig. 14. The ID carbide particles that remain undeformed impose constraint on their neighbouring dendrites and introduce local strain concentrations at their boundary to the adjacent dendrites, which ultimately lead to the ID decohesion.

Beaurin *et al.* [6] claimed that the metallurgical evolutions during the welding processes have very little influences on the final mechanical

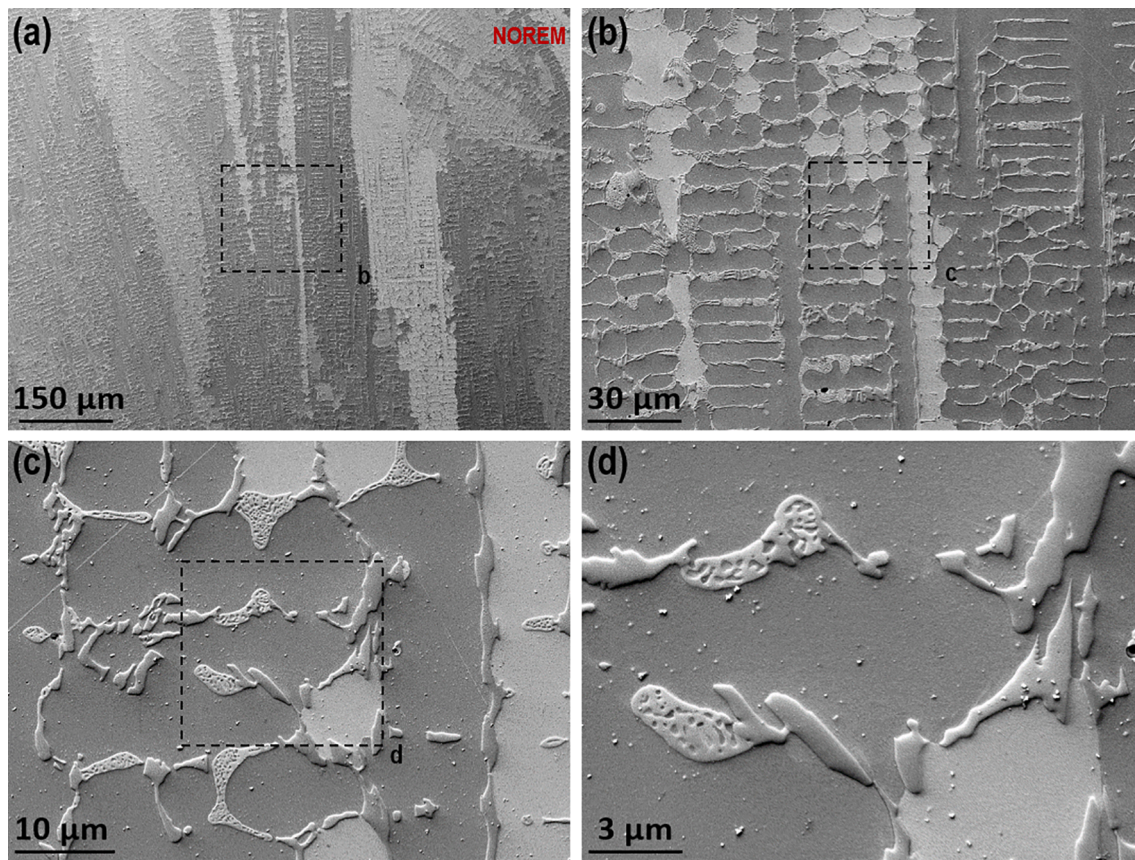


Fig. 11. (a-d) low kV SE images of the NOREM 02 hardfacing microstructure from a location far away from the main cracking. The austenitic dendrites were  $\sim 10 \mu\text{m}$  in size.

properties. However, as observed in this study, the metallurgical defects could also play a role in the failure. ID cavities/microcracks together with hard and brittle carbides may facilitate the cracking of NOREM 02 hardfacing. A high density of metallurgical defects with ID cavity clusters in hardfacing deposit were observed at locations close to HAZ and at the triple joint locations between weld beads and fusion boundary. The formation and opening of ID cavities/cracks in the hardfacing materials are probably related to a high level of residual tensile transient welding stresses after welding of the second layer of NOREM 02 deposit and the residual elements such as P and S.

The possible mismatch of the hardness and the dilatation coefficient between the NOREM 02 hardfacing and the stainless steel base metal (NOREM 02 has a lower dilatation coefficient than the austenitic valve body) also facilitates the cracking of NOREM 02, particularly along the fusion boundary. The cracks initiated at the fusion boundary and propagate towards the sealing/top surface and the fusion line. The radial cracks propagated throughout the thickness of NOREM 02 hardfacing along the ID boundaries. However, the crack stopped at the interface with the base material of stainless steel. The high ductility and fracture toughness and relatively low hardness of valve body made of austenitic stainless steel together with its microstructure (austenitic microstructure instead of ID network) resulted in the crack arrest.

#### Potential caution and mitigation

NOREM 02 has been considered and applied as a replacement of Co-containing alloys for stop and swing check valves, globe valves, and butterfly valves in NPPs [26]. When tested and applied at room temperature, LBW or PTAW processed NOREM 02 showed excellent friction and wear characteristics, similar to those of Stellites [27]. However, it exhibits an inferior galling wear performance and a rising coefficient of

friction at temperatures range above  $180 \text{ }^\circ\text{C}$  [10,28], since NOREM 02 cannot form the strain induced martensite like in Stellites in such temperatures and the stacking fault energy of NOREM 02 cannot be kept as the temperature increases [16]. Therefore, NOREM 02 is not suitable as a replacement of Stellites in NPP circuits at elevated temperatures [29]. Particular caution should be taken in specifying NOREM 02 for applications in gate valves that must meet stringent leakage requirements under high temperature and high differential pressure [17].

It has been reported that the microstructure and types of carbide in the Co-free hardfacing influence the tribological and mechanical properties [30]. Mathieu *et al.* reported that the NOREM sample subjected to the longer heat treatment at high temperature ( $\sim 1100 \text{ }^\circ\text{C}$ ) exhibited a drastic change in its microstructure, *i.e.* the disappearance of ferrite and the evolution of carbide population, due to diffusion mechanisms [31]. The cracking susceptibility of hardfacing can increase when the microstructure is lacking of ferrite, due to a better ductility of ferrite at high temperatures than austenite, permitting higher level of thermal stresses relaxation [22,32]. According to the WRC-1992 diagram [33], NOREM 02 welds generally solidify in a primary austenitic solidification structure with a low ferrite content. This accentuates the importance of extremely low P and S contents in preventing hot cracking. Thus, it is difficult to fully retard micro-cracks for a primary austenitic weld due to the high level of strain resulting from shrinkage. These cracks have been shown to occur along prior austenite GBs with a mechanism similar to the one result in hot cracking, where GB sliding and local strain promoted cracks to occur. The cracks mainly grew and propagated along ID boundaries of columnar ID carbides that are shortcut paths for cracks in NOREM 02 welds. The lacking of ferrites in the microstructure in the present case compared to the references [17,20,21] are potentially due to the difference in the contents of alloying elements and also the weld cooling parameters [34].

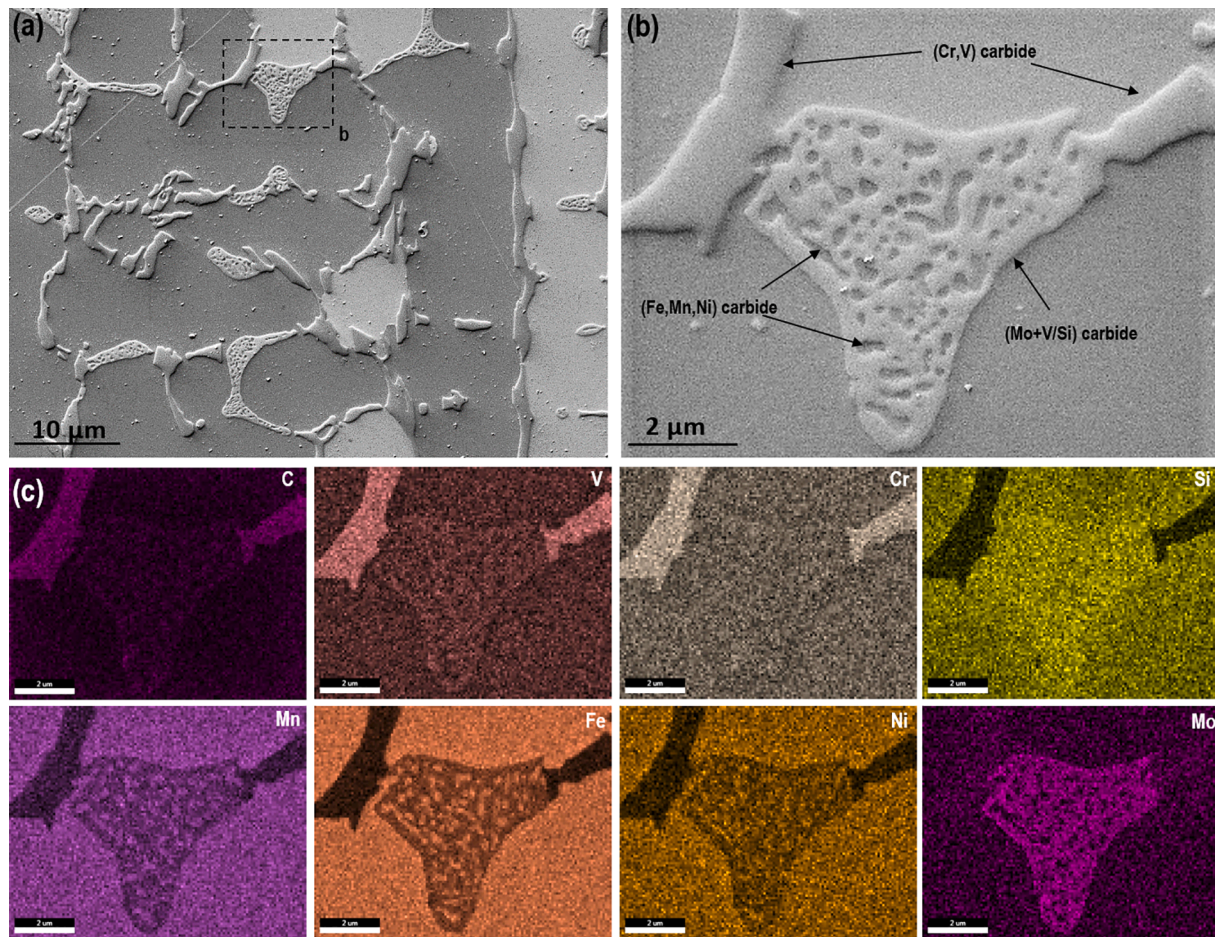


Fig. 12. (a-b) low kV SE images and (c) EDX mapping of the area in b.

Potential mitigation methods for the brittle cracking of NOREM hardfacing may include alloying design, deposition method and manufacturing parameters [25]. Tsai *et al.* reported that higher Mn and Mo contents can inhibit the solidification cracking of austenitic welds [32]. Reducing the contents of Si, P and S is generally known to decrease the hot cracking susceptibility. Regarding welding, low heat input together with a relatively high welding speed is considered as an effective approach for reducing micro-cracking by limiting the weld pool size and the extent to which underlying passes are heated. This stems from the observations that fissures found in austenitic welds occur mainly along the GBs of reheated weld metal (*i.e.* HAZ formed by subsequent passes) [35]. The fissuring propensity in austenitic weld metals can be enhanced by multiple thermal cycles; for instance, it has been observed that the amount of cracks in the HAZ (*i.e.* reheated weld metal) increased with the multiple thermal cycles experienced by the HAZ. Consequently, limiting the hardfacing thickness by using no more than three layers (passes), each of layer with no more than 1.6 mm thick, was reported by EPRI to reduce the cracking risk. It was also found that hardfacing deposits greater than 6–7 mm tend to develop greater stresses during plant application and thus the potential to crack occurrence is much greater. Despite low heat input, controlling the rate of weld cooling is important to control weld thermal gradients. Cool down rates can be lowered by using separate insulations or ramping down the pre-heating equipment *e.g.* 10 °C per hour. To protect the weld from cracking, a hammer peening process has sometimes been applied to mitigate the tensile stress by inducing a compressive stress layer on the weld surface [32]. Besnard *et al.* reported that NOREM 02 hardfacing prepared by hot isostatic pressing (HIP) exhibits better wear resistance than that by PTAW [36]. The fine microstructure obtained by HIP

procedure contain small globular carbides homogeneously distributed in the matrix [37] that allows the material to better withstand the external mechanical loads [36]. Smith *et al.* reported powder metallurgy hardfacing (up to 0.5 wt% N) can enhance both deformation-induced martensite transformation at room temperatures and deformation twinning at elevated temperatures [38]. These strain-hardening mechanisms, together with the increase in volume fraction of precipitates, effectively inhibit strain localization and enhance galling resistance up to 350 °C. Future application of HIP, powder metallurgy or a joint of both methods can be solutions for enhancing the galling wear performance of NOREM 02 or other Co-free hardfacing alloys at elevated temperature range in NPPs.

Moreover, the dye penetrant test in the factory acceptance test for the investigated valve was not able to reveal the potential manufacturing defects in the hardfacing, which emphasize a need for further developing and applying the reliable non-destructive evaluation methods, *e.g.* ultrasonic testing and eddy current methods on hardfacing alloys.

## Conclusions

Detailed failure analysis and microstructural study of a nuclear swing check plug valve with through-the-thickness cracks in the Co-free hardfacing deposit with NOREM 02 were performed.

- The solidification defects and the lacking of ferrite phase in the microstructure together with residual stresses and the potentially non-optimized thermal treatments are the causes of the cracking.

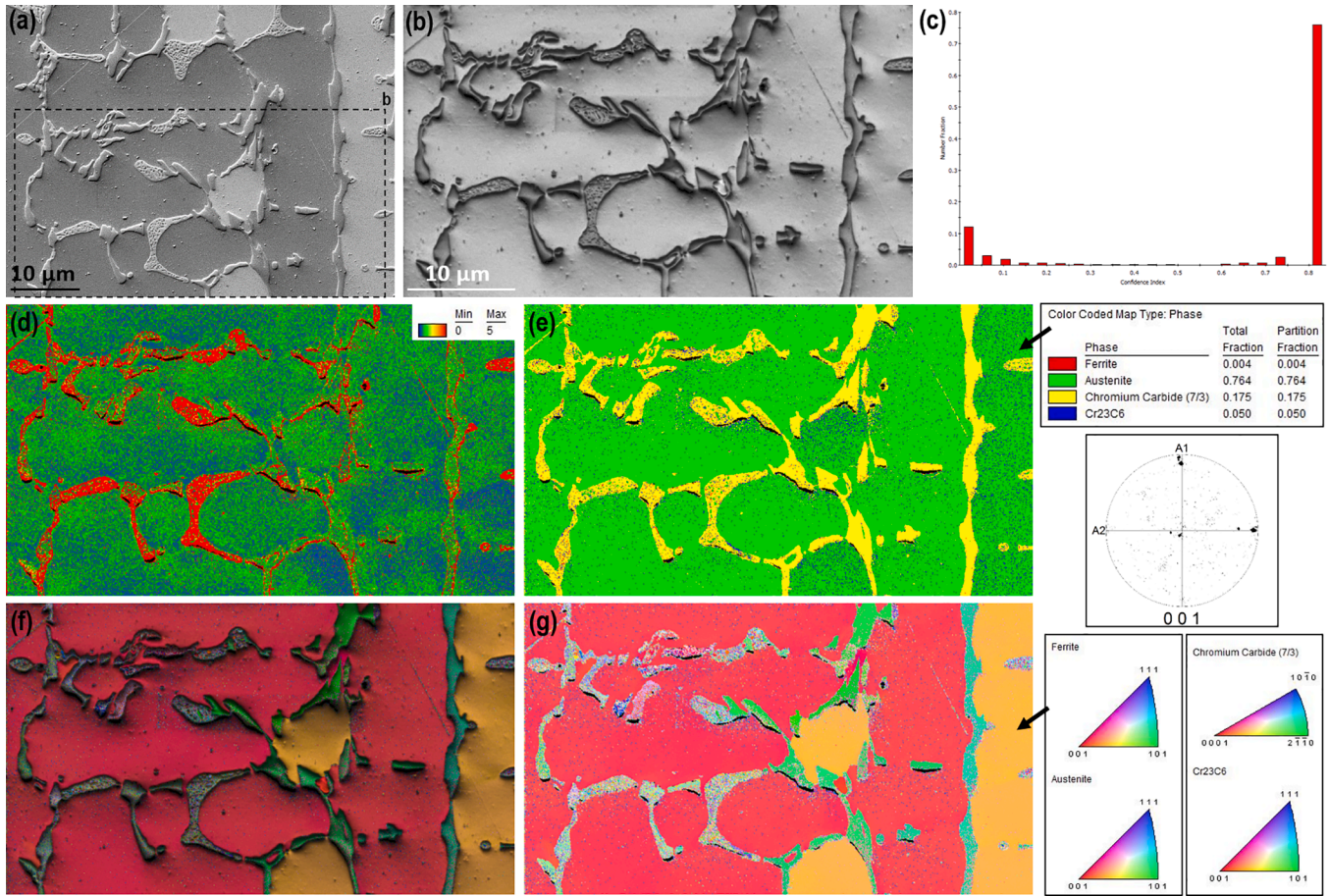


Fig. 13. (a) low kV SE image, (b) IQ image, (c) correlation of number fraction with coincidence index, (d) KAM map, (e) phase map, (f) IQ + IPF and (g) IPF image.

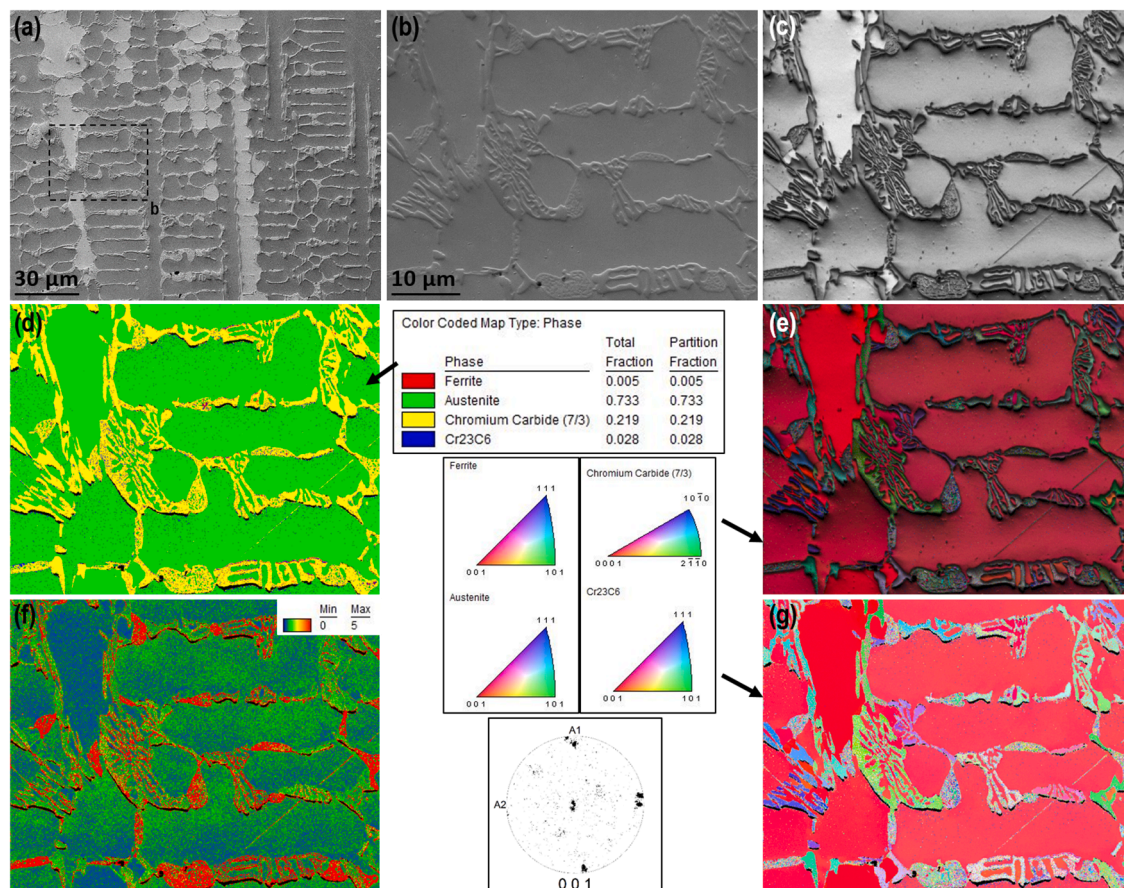


Fig. 14. (a) low kV SE image, (b) high kV SE image, (c) IQ image, (d) phase map, (e) IQ + IPF, (f) KAM map and (g) IPF image. (b-g) are from the area with inset in (a).

- ID cavities associated with brittle carbides under the residual stresses facilitated the propagation of cracking in NOREM O2. Dendrite packages perpendicular to the main stress direction was most prone to cracking.
- The mismatch of the hardness and the dilatation coefficient between the NOREM O2 hardfacing and the base metal may play additional role.
- NOREM O2 hardfacing has a dendritic austenitic matrix with ID network of carbides of M7C3 type. Eutectic carbides rich in Fe-Mn-Ni and Mo-V-Si and non-eutectic carbides rich in Cr-V were found.

#### CRediT authorship contribution statement

**Zaiqing Que:** Conceptualization, Data curation, Formal analysis, Investigation, Methodology, Project administration, Resources, Writing – original draft, Writing – review & editing. **Matias Ahonen:** Conceptualization, Data curation, Formal analysis, Investigation, Methodology, Writing – original draft. **Iikka Virkkunen:** Project administration, Resources, Supervision, Writing – review & editing. **Pekka Nevasmaa:** Supervision, Writing – review & editing. **Paavo Rautala:** Resources, Writing – review & editing. **Hannu Reinvald:** Resources, Writing – review & editing.

#### Declaration of Competing Interest

The authors declare that they have no known competing financial interests or personal relationships that could have appeared to influence the work reported in this paper.

#### Acknowledgements

The work is supported by customer research project 118577 NOR-EM02\_MP funded by Teollisuuden Voima Oyj and SAFIR 2022 NOCO+ (Cobalt-free hardfacings) project. The authors would like to express their gratitude for the experimental contributions from T. Lehtikuusi and J. Lukin of VTT. The authors would like to thank A. Forsström, U. Ehrnstén and H. Hänninen for support.

#### References

- [1] H. Ocken, The galling wear resistance of new iron-based hardfacing alloys: a comparison with established cobalt- and nickel-base alloys, *Surf. Coat. Technol.* 76–77 (1995) 456–461.
- [2] P. Aaltonen, U. Ehrnstén, P. Karjalainen-Roikonen, J.-M. Autio, T. Saukkonen and H. Hänninen, “Ageing degradation of a hard-facing alloy after long-time exposure to BWR conditions,” in: *16th International Conference on Environmental Degradation of Materials in Nuclear Power Systems and Water Reactors*, Ashville, North Carolina, USA, 2013.
- [3] C.B. Bahn, B.C. Han, J.S. Bum, I.S. Hwang, C.B. Lee, Wear performance and activity reduction effect of Co-free valves in PWR environment, *Nucl. Eng. Des.* 231 (1) (2004) 51–65.
- [4] P. Aubry, C. Blanc, I. Demirci, M. Dal, T. Malot, H. Maskrot, Analysis of nickel based hardfacing materials manufactured by laser cladding for sodium fast reactor, *Physics Procedia* 83 (2016) 613–623.
- [5] R. Smith, “Development of a nitrogen-modified stainless-steel hardfacing alloy,” Doctoral dissertation, Ohio State University, 2015.
- [6] G. Beaurin, J.-P. Mathieu, E. Gauthier, D. Nelias, Microstructural and mechanical properties evolutions of plasma transferred arc deposited Norem02 hardfacing alloy at high temperature, *Mater. Sci. Eng., A* 528 (15) (2011) 5096–5105.
- [7] “Occupational exposures at nuclear power plants, Twenty-fifth annual report of the ISE programme,” OECD Nuclear Energy Agency, 2015.
- [8] B. Cockeram, R. Buck, W. Wilson, Laboratory galling tests of several commercial cobalt-free weld hardfacing alloys, *Surf. Coat. Technol.* 94–05 (1997) 495–500.

- [9] M. Keränen, "Effect of welding parameters on plasma transferred arc welding method on abrasive wear resistance of 12V tool steel deposit", Doctoral Dissertations 220, Aalto University, Espoo, 2010.
- [10] J. Kim, S. Kim, The temperature dependence of the wear resistance of iron-based NOREM 02 hardfacing alloy, *Wear* 237 (2000) 217–222.
- [11] D.H.E. Persson, S. Jacobson, S. Hogmark, Effect of temperature on friction and galling of laser processed Norem 02 and Stellite 21, *Wear* 255 (1-6) (2003) 498–503.
- [12] B. Cockeram, Laboratory testing of several commercial cobalt-free weld hardfacing alloys, *Surf. Coat. Technol.* 94–95 (1997) 495–500.
- [13] M. Carnus, X. Confort, "Replacement of Cobalt base alloys hardfacing by NOREM alloy; EDF experience and development, some metallurgical considerations Valve application (CLAMA, RAMA)," in *Fontevraud* 7, 2010.
- [14] A. Ross, "Compilation and Evaluation of NOREM Test Results: Implications for Valve Applications," EPRI Report TR-109343, Palo Alto, CA, USA, 1999.
- [15] K. Smith, "Performance of NOREM Hardfacing: In-Situ Application and Leak Rate Testing of," EPRI Report TR-107987, Palo Alto, CA, USA, 1997.
- [16] F. Delcer, "Monitoring Performance of Valves with NOREM Hard Facing," EPRI Report TR-109345, Palo Alto, CA, USA, 1998.
- [17] H. Ocken, "Performance of Norem Hardfacing Alloys," EPRI Report TR-112993-1999, Palo Alto, CA, USA, 1999.
- [18] R. Shen, P. Efsing, Overcoming the drawbacks of plastic strain estimation based on KAM, *Ultramicroscopy* 184 (2018) 156–163.
- [19] Z. Que, H. Seifert, V. Mazánová and P. Spätig, "Hydrogen embrittlement on fracture resistance of low-alloy reactor pressure vessel steel with high dynamic strain aging at 288 °C," *Materials Letters*, vol. 308, no. 131269, 2022.
- [20] E.K. Ohriner, T. Wada, E.P. Whelan, H. Ocken, The chemistry and structure of wear-resistant, iron-base hardfacing alloys, *Metall. Mater. Trans.* 22 (5) (1991) 983–991.
- [21] B. Cockeram, Some observations of the influence of  $\delta$ -ferrite content on the hardness, galling resistance, and fracture toughness of selected commercially available iron-based hardfacing alloys, *Metall. Mater. Trans.* 33 (2002) 3403–3419.
- [22] V. Shankar, T.P.S. Gill, S.L. Mannan, S. Sundaresan, Solidification cracking in austenitic stainless steel welds, *Sadhana* 28 (3-4) (2003) 359–382.
- [23] N. Sridharan, E. Cakmak, R. Dehoff, Microstructure evolution during laser direct energy deposition of a novel Fe-Cr-Ni-W-B hardfacing coating, *Surf. Coat. Technol.* 358 (2019) 362–370.
- [24] J. Siefert, S. David, Weldability and weld performance of candidate austenitic alloys for advanced ultrasupercritical fossil power plants, *Sci. Technol. Weld. Joining* 19 (4) (2014) 271–294.
- [25] A. Nazarko, R. Plomodyalo, Influence of chemical composition of wear-resistant hard-facing materials on the tendency to formation of hot cracks during weld facing, *Mater. Today: Proc.* 19 (2019) 2422–2424.
- [26] K.-Y. Lee, G.G. Kim, J.H. Kim, S.-H. Lee, S.-J. Kim, Sliding wear behavior of hardfacing alloys in a pressurized water environment, *Wear* 262 (7-8) (2007) 845–849.
- [27] J. Vikström, Galling resistance of hardfacing alloys replacing Stellite, *Wear* 179 (1-2) (1994) 143–146.
- [28] B. Cockeram, Fracture toughness testing and toughening mechanisms of some commercial cobalt-free hardfacing alloys, *Surf. Coat. Technol.* 108–109 (1998) 377–384.
- [29] N.-R. Park, D.-G. Ahn, Wear characteristics of Stellite 6 and Norem 02 hardfacing SKD61 hot working tool steel at the elevated temperature, *Int. J. Precis. Eng. Manuf.* 15 (2014) 2549–2558.
- [30] S. Pawar, A. Jha, G. Mukhopadhyay, Effect of different carbides on the wear resistance of Fe-based hardfacing, *Int. J. Refract. Metals* 78 (2019) 288–295.
- [31] J. Mathieu, F. Arnoldi, E. Gauthier and G. Beaurin, "Modelling of residual stresses in valves Norem hard-facing alloys: A material characterization issue," in *Fontevraud* 7, 2010.
- [32] K. Tsai, S. Jeng, J. Huang, Prevention of delayed cracking of iron based hardfacing welds, *Eng. Fail. Anal.* 48 (2015) 210–217.
- [33] D. Kotecki, T. Siewert, WRC-1992 Constitution Diagram for Stainless Steel Weld Metals: A Modification of the WRC-1988 Diagram, *Welding Research Supplement* (1992) 171–178.
- [34] N. Çomez, C. Çivi, H. Durmuş, Reliability evaluation of hardness test methods of hardfacing coatings with hypoeutectic and hypereutectic microstructures, *Int. J. Miner. Metall. Mater.* 26 (12) (2019) 1585–1593.
- [35] C.D. Lundin, D.F. Spond, "The nature and morphology of fissures in austenitic stainless steel weld metals," in: *AWS 57th Annual Meeting*, St. Louis, Missouri, 1976.
- [36] M. Ardigo-Besnard, A. Tellier, A. Besnard and J. Chateau-Cornu, "Effect of the microstructure on the tribological properties of HIPed and PTA-welded Fe-based hardfacing alloy," *Surface & Coatings Technology*, vol. 425, no. 127691, 2021.
- [37] C. Zhao, D. Stewart, J. Jiang, F. Dunne, A comparative assessment of iron and cobalt-based hard-facing alloy deformation using HR-EBS and HR-DIC, *Acta Mater.* 159 (2018) 173–186.
- [38] R. Smith, M. Doran, D. Gandy, S. Babu, L. Wu, A. Ramirez, P. Anderson, Development of a gall-resistant stainless-steel hardfacing alloy, *Mater. Des.* 143 (2018) 38–48.